Available online at www.sciencedirect.com
SCIENCE DIRECT®
Acta Materialia 52 (2004) 3313–3322
Acta MATERIALIA
www.actamat-journals.com

X-ray diffraction measurement of residual stress in PZT thin films prepared by pulsed laser deposition

Xuejun Zheng [a,b,*], Jiangyu Li [c], Yichun Zhou [a,b]

[a] Institute of Fundamental Mechanics and Materials Engineering, Xiangtan University, Xiangtan, Hunan 411105, PR China
[b] Faculty of Material Photoelectronic Physics, Xiangtan University, Xiangtan, Hunan 411105, PR China
[c] Department of Engineering Mechanics, University of Nebraska – Lincoln, Lincoln, NE 68588-0526, USA

Received 5 September 2003; received in revised form 10 February 2004; accepted 12 February 2004
Available online 20 April 2004

Abstract

Based on piezoelectric constitutive equations and Bragg law, we proposed an extended model, in which the piezoelectric coupling factor determined by the elastic, dielectric and piezoelectric constants is introduced, to evaluate the residual stress in ferroelectric thin film with X-ray diffraction (XRD). $Pb(Zr_{0.52}Ti_{0.48})O_3$ thin films with thickness 0.05, 0.5, and 1.0 μm were grown on Pt/Ti/Si(0 0 1) by pulsed laser deposition (PLD) at the substrate temperature 650 °C and oxygen pressure 40 Pa. D500 goniometer and $\sin^2\psi$ method were used to measure the residual stress in PZT thin films. The origin of residual stress was theoretically discussed from the epitaxial stress, intrinsic stress, thermal stress, and transformation stress. The results show that the theoretical results are closer to the experimental results evaluated by the extended model, and the residual compressive stress evaluated by the extended model is larger than that evaluated by the conventional model due to the consideration of the piezoelectric coupling effects.

Keywords: Piezoelectricity; PZT thin film; X-ray diffraction; Residual stress

1. Introduction

The rapid growth of the field of microelectromechanical systems (MEMS) has generated intense research activities [1–3] to develop techniques for the characterization of the mechanical properties such as elastic modulus, hardness, interface adhesion, and residual stress for thin film materials [4–6]. Lead–zirconate–titanate $Pb(Zr_xTi_{1-x})O_3$ (PZT) is considered to be an important ferroelectric thin film material and has developed rapidly in recent years due to its potential applications [7,8], since it has high piezoelectric coefficients and low dielectric coefficients [9,10]. The residual stresses will be produced inevitably in thin film due to the structural misfit and thermal misfit of the thin films/substrate and the process from high temperature to low temperature during the deposition of thin films [11,12]. Much research has shown that the residual compressive stress may cause the film delamination from the substrate and the residual tensile stress may cause the surface crack in films [13,14]. Obviously, residual stress in thin films has important effects on the film's service life, and the determination of residual stress in ferroelectric thin films is indispensable.

Several techniques such as nano-indentation fracture method [5], X-ray diffraction [6], and Raman spectroscopy [15] were used to measure residual stresses in PZT thin films. However, as we know, it is possibly incorrect to evaluate the residual stresses in ferroelectric thin films by the conventional model of XRD measurement [6,16], where thin films are assumed as isotropic and the piezoelectric coupling effects are neglected. In the paper, we proposed an extended model to evaluate residual stresses in ferroelectric thin films with X-ray diffraction. In order to understand the effects of anisotropy and piezoelectric coupling of ferroelectric thin films on residual stress, the measured results of the extended model were

* Corresponding author. Tel.: +86-732-8293648; fax: +86-732-8292468.
E-mail addresses: xj_zheng2002@hotmail.com, zhengxuejun@xtu.edu.cn (X. Zheng).

1359-6454/$30.00
doi:10.1016/j.actamat.2004.02.047

compared with that of the conventional results for PZT thin films grown on Pt/Ti/SiO_2/Si(0 0 1) by PLD. On the other hand, the theoretical models [11,12], in which thin films are considered as isotropic materials, were used to discuss the origin of residual stress in ferroelectric thin film. It is very important to answer whether there are larger residual stresses in ferroelectric thin films due to the anisotropy and piezoelectric coupling effects, and whether the measured residual stresses of the extended model are closer to the true values than that of the conventional model.

2. Model

2.1. Bragg diffraction

X-ray techniques provide one of the non-destructive methods of measuring residual stresses [6,16]. X-ray stress (strain) analysis is based on the Bragg diffraction equation

$$n\lambda = 2d\sin\theta, \tag{1}$$

where n is an integer (diffraction order), λ the wavelength of the incident X-ray, d the interplanar spacing of the polycrystalline material under consideration, and θ is the Bragg angle (see Fig. 1). A change in the interplanar spacing Δd will produce a corresponding change in the Bragg angle, $\Delta\theta$, such that lattice strain can be expressed from

$$\frac{\Delta d}{d_0} = \varepsilon = -\cot(\theta)\Delta\theta = -\cot(\theta)\frac{\Delta(2\theta)}{2}, \tag{2}$$

where d_0 is the unstrained lattice spacing, ε is the mechanical strain, and $\Delta\theta$ is the change in Bragg diffraction orientation due to the strain. When diffraction occurs, Eqs. (1) and (2) relate lattice strain in the arbitrary orientation defined by angles ψ and ϕ of Fig. 2 to the change in Bragg diffraction orientation $\Delta\theta$. The atomic planes defining the gage length are perpendicular to the

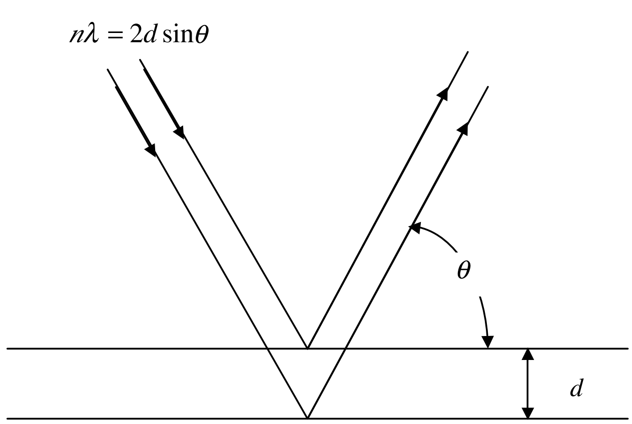

Fig. 1. Bragg diffraction at point p.

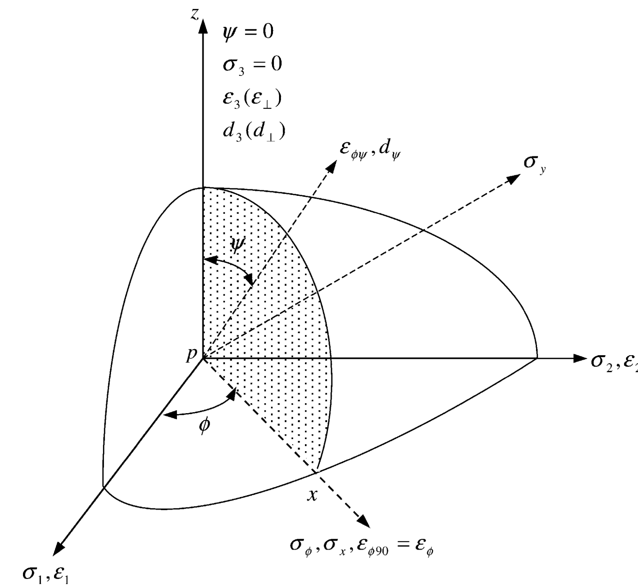

Fig. 2. Stress and stress ellipsoids at point p.

incident and diffracted beam bisector, while it is the normal strain along this bisector that is measured at point p of Fig. 1. If $d_\perp$ and d_ψ are the measured spacing of atomic planes parallel to the surface and with orientations ψ of the z–x plane in the strained state, the strain normal to the surface and the normal strain in the z–x plane are

$$\varepsilon_\perp = \varepsilon_3 = \varepsilon_{\phi 0} = \frac{d_\perp - d_0}{d_0} \quad \text{and} \quad \varepsilon_{\phi\psi} = \frac{d_\psi - d_0}{d_0},$$

respectively [6,17]. Then

$$\varepsilon_{\phi\psi} - \varepsilon_3 = \frac{d_\psi - d_\perp}{d_0} \approx \frac{d_\psi - d_\perp}{d_\perp} = -(\theta_\psi - \theta_\perp)\cot\theta_0, \tag{3}$$

where $\theta_\perp$ and θ_ψ are the measured Bragg diffraction angles at $\psi = 0$ and $\psi \neq 0$, respectively. $\cot\theta_0$ is considered as a constant.

2.2. Stress–strain analysis

Stress and strain at point p under investigation can be obtained from X-ray data with the aid of the stress and strain ellipsoids (Fig. 2). Principal strains ε_1 and ε_2 are assumed to lie in the plane of the material and ε_3 normal to the plane. From strain transformation and the angles of Fig. 2, the normal strain $\varepsilon_{\phi\psi}$ in the z–x plane is given by

$$\varepsilon_{\phi\psi} = \varepsilon_1\alpha_1^2 + \varepsilon_2\alpha_2^2 + \varepsilon_3\alpha_3^2, \tag{4}$$

where the direction cosines are given by

$$\begin{aligned} \alpha_1 &= \cos\phi\sin\psi, \\ \alpha_2 &= \sin\phi\sin\psi, \\ \alpha_3 &= \cos\psi = \sqrt{1 - \sin^2\psi}. \end{aligned} \tag{5}$$

Eqs. (4) and (5) are combined to give

$$\frac{\varepsilon_{\phi\psi} - \varepsilon_3}{\sin^2\psi} + \varepsilon_3 = \varepsilon_1 \cos^2\phi + \varepsilon_2 \sin^2\phi. \tag{6}$$

Similarly, the stress component σ_ϕ in the plane of the material ($\psi = \pi/2$) can be written in terms of the principal stresses σ_1, σ_2, and in-plane angle ϕ as

$$\sigma_\phi = \sigma_1 \cos^2\phi + \sigma_2 \sin^2\phi. \tag{7}$$

2.3. Piezoelectric constitutive relationship

We first present a general theory for the transversely isotropic piezoelectric solids, governed by the following constitutive equations [5]:

$$\begin{aligned}
\sigma_1 &= c_{11}\varepsilon_1 + c_{12}\varepsilon_2 + c_{13}\varepsilon_3 - e_{31}E_z,\\
\sigma_2 &= c_{12}\varepsilon_1 + c_{11}\varepsilon_2 + c_{13}\varepsilon_3 - e_{31}E_z,\\
\sigma_3 &= c_{13}\varepsilon_1 + c_{13}\varepsilon_2 + c_{33}\varepsilon_3 - e_{33}E_z,\\
D_z &= e_{31}\varepsilon_1 + e_{31}\varepsilon_2 + e_{33}\varepsilon_3 + \epsilon_{33}E_z,
\end{aligned} \tag{8}$$

where D_z, E_z are the electric displacement and electric field in the polar direction z normal to the plane, $c_{11}, c_{12}, c_{13}, c_{33}$ are the elastic constants, e_{31}, e_{33} are the dielectric constants, and ϵ_{33} is the piezoelectric constant, respectively. At a stress-free surface of the thin film, the stress and electric boundary conditions are given as

$$\sigma_3 = 0, \quad D_z = 0. \tag{9}$$

Substituting them into last two equations of Eqs. (8) yields

$$E_z = \frac{(c_{33}e_{31} - e_{33}c_{13})}{(e_{33}e_{31} + c_{13}\epsilon_{33})}\varepsilon_3, \tag{10}$$

$$(\varepsilon_1 + \varepsilon_2) = -\frac{(c_{33}\epsilon_{33} + e_{33}^2)}{(c_{13}\epsilon_{33} + e_{31}e_{33})}\varepsilon_3. \tag{11}$$

Eqs. (8), (10), and (11) are substituted into Eq. (7), resulting in (see Appendix A)

$$\begin{aligned}
&\sigma_\phi + \frac{c_{12}(c_{33}\epsilon_{33} + e_{33}^2) + e_{31}^2 c_{33} - 2c_{13}e_{31}e_{33} - c_{13}^2\epsilon_{33}}{c_{13}\epsilon_{33} + e_{31}e_{33}}\varepsilon_3\\
&\quad = (c_{11} - c_{12})(\varepsilon_1 \cos^2\phi + \varepsilon_2 \sin^2\phi)
\end{aligned} \tag{12}$$

so that Eqs. (6) and (12) can be expressed as

$$\begin{aligned}
&\frac{(c_{11} - c_{12})(\varepsilon_{\phi\psi} - \varepsilon_3)}{\sin^2\psi}\\
&\quad = \sigma_\phi + \left[((c_{12}(c_{33}\epsilon_{33}) + e_{33}^2) + e_{31}^2 c_{33} - 2c_{13}e_{31}e_{33} - c_{13}^2\epsilon_{33})\right.\\
&\qquad \left./(c_{13}\epsilon_{33} + e_{31}e_{33}) - c_{11} + c_{12}\right]\varepsilon_3.
\end{aligned} \tag{13}$$

Substituting Eqs. (10) and (11) into first two equations of Eqs. (8) yields (see Appendix B)

$$\begin{aligned}
&\sigma_1 + \sigma_2\\
&\quad = [4c_{13}e_{31}e_{33} + 2c_{13}^2\epsilon_{33} - 2e_{31}^2 c_{33} - (c_{11} + c_{12})(c_{33}\epsilon_{33} + e_{33}^2)]\\
&\qquad /(c_{13}\epsilon_{33} + e_{31}e_{33})\varepsilon_3.
\end{aligned} \tag{14}$$

2.4. Residual stress of ferroelectric thin film

It is assumed that the surface of a transversely isotropic thin film has been subjected to prior mechanical and/or thermal loading which include: (i) non-uniform cooling from the processing temperature; (ii) deposition of a surface coating or a thin film on a substrate by thermal spray, sputtering, physical vapor deposition (PVD), chemical vapor deposition (CVD) or molecular beam epitaxy (MBE); and (iii) phase transformation. Such history is assumed to result in an equal-biaxial state of residual stress (tensile or compressive) whose magnitude at the surface is uniform over a certain indentation depth [17,18]. Then

$$\sigma_1 = \sigma_2 = \sigma_\phi. \tag{15}$$

Substituting Eqs. (14) and (15) into Eq. (13), one can obtain (see Appendix C)

$$\sigma_\phi = \chi\frac{(\varepsilon_{\phi\psi} - \varepsilon_3)}{\sin^2\psi}, \tag{16}$$

where the piezoelectric coupling factor is defined as

$$\chi = \frac{(c_{11} + c_{12})(c_{33}\epsilon_{33} + e_{33}^2) - 4c_{13}e_{31}e_{33} - 2c_{13}^2\epsilon_{33} + 2e_{31}^2 c_{33}}{2(c_{13}\epsilon_{33} + e_{31}e_{33}) + (c_{33}\epsilon_{33} + e_{33}^2)}. \tag{17}$$

From Eqs. (3) and (16), the change of strain $\varepsilon_{\phi\psi} - \varepsilon_3$ is liner with $\sin^2\psi$, and the relationship between the slope $\partial(2\theta)/\partial(\sin^2\psi)$ and the residual stress σ_ϕ is

$$\sigma_\phi = \chi \cot\theta_0 \frac{\pi}{360}\frac{\partial(2\theta)}{\partial(\sin^2\psi)} \tag{18}$$

with angle θ expressed in degrees. Experiments show that the relationship between 2θ (or$\varepsilon_{\phi\psi} - \varepsilon_3$) and $\sin^2\psi$ is indeed linear. Practically by measuring different diffraction line displacement under different ψ, and plotting 2θ as a function of $\sin^2\psi$, the residual stress in the thin film can be obtained by the slope of $2\theta - \sin^2\psi$ line.

3. Experimental

3.1. Sample preparation

In the deposition of PZT thin films, the PZT bulk ceramic with morphotropic composition Zr/Ti = 52/48 was used as a target, KrF pulsed laser as an evaporate source, oxygen as ambient gas in the vacuum chamber. The irradiation was performed in a stainless steel vacuum chamber and the laser beam from KrF laser, with wavelength of 248 nm, pulsed width of 30 ns, frequency of 5 Hz, and laser energy of 1.5 J/cm^2, was focused on the PZT ceramic target. Pt/Ti/Si(0 0 1) substrate with plane-sizes 10×10 mm^2 was composed of Pt bottom electrode (thickness 200 nm), Ti transition-layer (thickness 150 nm), and Si(0 0 1) substrate (thickness 2 mm).

The distance between target and substrate was fixed at 60 mm. The laser beam was incident on surface of the target at an angle of 45°. During irradiation, the target was rotated with a constant speed of 5 r/min in order to avoid crater formation. The oxygen pressure was about 30 Pa and the substrate temperature was set as 650 °C. PZT thin films with different thickness 0.05, 0.5, and 1.0 μm were prepared by controlling the deposition time. In order to determine the *c*-axis lattice constant of PZT thin film in tetragonal phase at room temperature, the deposited thin films with different thickness were annealed at 650 °C with 10 min. After X-ray diffraction analyses, the sample surfaces were eroded by the diluted hydrochloric acid in order to observe the grain sizes.

3.2. Measurement of XRD and surface profile

The Siemens D500 X-ray diffractometer with Cu Kα radiation was used to analyze the crystalline phases in PZT thin films before and after annealing. The X-ray radiation source of Cu Kα with a wavelength of 1.5406 nm was adopted at 36 kV and 30 mA. The scanning angle was in the region of 20–70°, the (1 1 0) and (0 0 2) planes of PZT thin films were scanned at 4°/min and the degree increment was 0.02°. D500 texture goniometer equipped with a Cu tube and an open Eulerian cradle was used to measure angles θ and their changes with orientations ψ. The (2 0 2) planes of PZT thin films were scanned at 0.25°/min and the degree increment of 0.01° using XRD with a monochromatic Cu Kα generated at 40 kV and 40 mA. The sample surfaces eroded by the diluted hydrochloric acid were observed by S-750 scanning electron microscopy (SEM).

3.3. The determination of parameters

To determine necessary parameters for XRD measurement of residual stresses in PZT thin films, we used the elastic, piezoelectric and dielectric constants from [5]. Generally, the higher the diffraction angle 2θ, the more accurate the measurement is. Typically, residual stress is measured by diffractions that occur at more than 130° in 2θ angle to evaluate the residual stress. In the tests, when the scanning angles were in the region of 0–140°, the diffractions occurred at around 22°, 30°, 40°, 44°, 54°, 57°, 65° and 70° in 2θ angle. Because of the polycrystalline nature and the effect of substrate Si(0 0 4), the diffraction peak occurred at around 70° in 2θ angle was inappropriate to evaluate the residual stress. Therefore, Bragg's angle $2\theta_0$ at diffraction peak in the samples without residual stress is considered as a constant of 64.68°. They are listed in Table 1. In the theoretical analysis and discussions, ferroelectric thin films were assumed as isotropy and without piezoelectric coupling effects [11,12]. Poisson's ratio, elastic modulus and the thermal expansion coefficient of PZT thin film are obtained from [5,19] and the thermal expansion coefficient of substrate Si from [11], all of them are also listed in Table 1. The *c*-axis lattice constant of PZT thin film in tetragonal phase at room temperature before and after annealing are, respectively, calculated by the peaks on (0 0 2) plane of the sample in the investigation. The *a*-axis lattice constant of PZT thin film with thickness 1.0 μm before annealing is approximately 4.017 Å, same as bulk PZT materials [20,21]. Because the lattice constants of ferroelectric thin film are larger than those of bulk materials [11], they are assumed as 4.029 and 4.030 Å for PZT thin films with thickness 0.5 and 0.05 μm, respectively. The lattice constants of PZT film at cubic structure, electrode Pt and substrate Si are obtained from [11,21,22], respectively. All those lattice constants are listed in Table 2.

4. Results and discussions

4.1. Microstructure, orientation and surface profile

The XRD patterns of PZT thin films deposited by the PLD method are shown in Fig. 3. The obvious diffraction peaks of PZT perovskite structure in the range of XRD resolution indicate that a lot of perovskite crystals are formed in PZT thin film with different film thickness of 0.05, 0.5 and 1.0 μm. In fact, it is very difficult to determine the crystal structure of PZT thin films near the morphotropic phase boundary (MPB). The splitting peaks such as (0 0 1)/{(1 0 0)(0 1 0)}, {(1 0 1)(0 1 1)}/(1 1 0), (0 0 2)/{(2 0 0)(0 2 0)}, (1 0 2)/{(2 0 1)(2 1 0)}, {(2 1 1)(1 2 1)}/(1 1 2), and {(2 0 2)(0 2 2)}/(2 2 0) doublets are often observed on XRD patterns of tetragonal structure for PZT thin films. However, the peak splitting is disappeared at the different orientations such as (1 0 0), (1 1 0), (0 0 2), (2 0 1), (1 1 2) and (2 0 2) on the XRD diagrams of the PZT thin films Zr/Ti = 52/48. Similar to experimental

Table 1
The materials parameters of PZT thin film

Elastic coefficients (10^{10} N m^{-2})				Piezoelectric coefficients (C m^{-2})			Dielectric coefficients (10^{-10} F m^{-1})	Thermal expansion coefficients (10^{-6}/K)		Poisson's ratio	Elastic modulus (10^{10} N m^{-2})
c_{11}	c_{33}	c_{13}	c_{12}	e_{15}	e_{13}	e_{33}	ϵ_{33}	α_f	α_s	v_f	E_f
13.9	11.5	7.43	7.78	12.7	−5.2	15. 1	15.1	7	3.5	0.3	13

Table 2
The lattice constants (Å) of PZT thin film and substrate

	c-axis		a-axis [11,20,21]	Film at cubic structure [21]	Substrate	
	Before annealing	After annealing			Pt [22]	Si [11]
$h_1 = 0.05$ μm	4.0958	4.0896	4.030	4.05	3.950	5.431
$h_2 = 0.5$ μm	4.0861	4.0804	4.029	4.05	3.950	5.431
$h_3 = 1.0$ μm	4.0817	4.0774	4.017	4.05	3.950	5.431

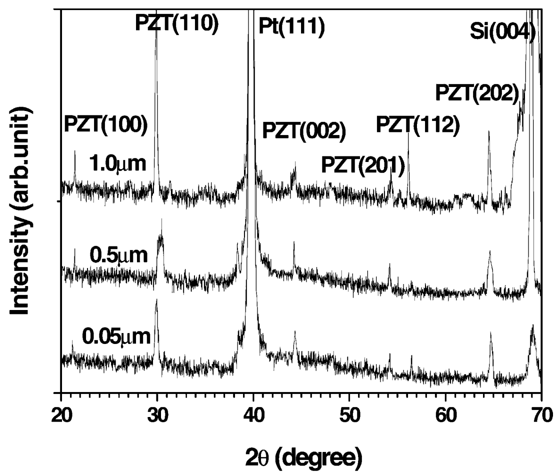

Fig. 3. XRD patterns of PZT thin film with different film thickness.

results given in [23], this splitting can be described as simple peak splitting of the cubic structure appearing at a temperature higher than the Curie temperature, therefore the films were considered as tetragonal in the paper. It is obvious that there is a lack of precision in the structural data obtained from PZT52/48 thin film diffractograms due to very low tetragonality of its structure hidden by the effect of size defects (peak broadening).

From Fig. 3, PZT films deposited by PLD on Pt/TiO_2/SiO_2/Si(0 0 1) are polycrystalline and the X-ray diffraction scans show the contribution of several film orientations, namely $\langle 100\rangle$, $\langle 110\rangle$, $\langle 002\rangle$, $\langle 201\rangle$, $\langle 112\rangle$, and $\langle 202\rangle$. The overlapped peaks lead to peak broadening. These films possessed preferential crystal orientation and the preferred (1 1 0) orientation decreased with increasing film thickness. The relative domain population corresponding to the (klm)-oriented area, which represents the degree of different orientation, can be represented as follows [24]:

$$P_{(klm)} = (I(klm))/(I(100) + I(110) + I(002) + I(201) + I(112) + I(202)), \tag{19}$$

where $I(klm)$ represents the XRD intensity of the (klm) reflection. The peaks on (1 1 0) and (0 0 2) planes of PZT thin film before annealing are given in Figs. 4(a) and (b). The relative domain population $P_{(klm)}$ corresponding to (1 0 0), (1 1 0), (0 0 2), (2 0 1), (1 1 2) and (2 0 2)-oriented area can be determined by XRD diagrams such as Figs. 4(a) and (b), and the results are listed in Table 4. The peaks on (0 0 2) plane of PZT thin films with different film thickness after annealing are given in Fig. 4(c). According the XRD data, the c-axis lattice parameters of PZT thin film before and after annealing

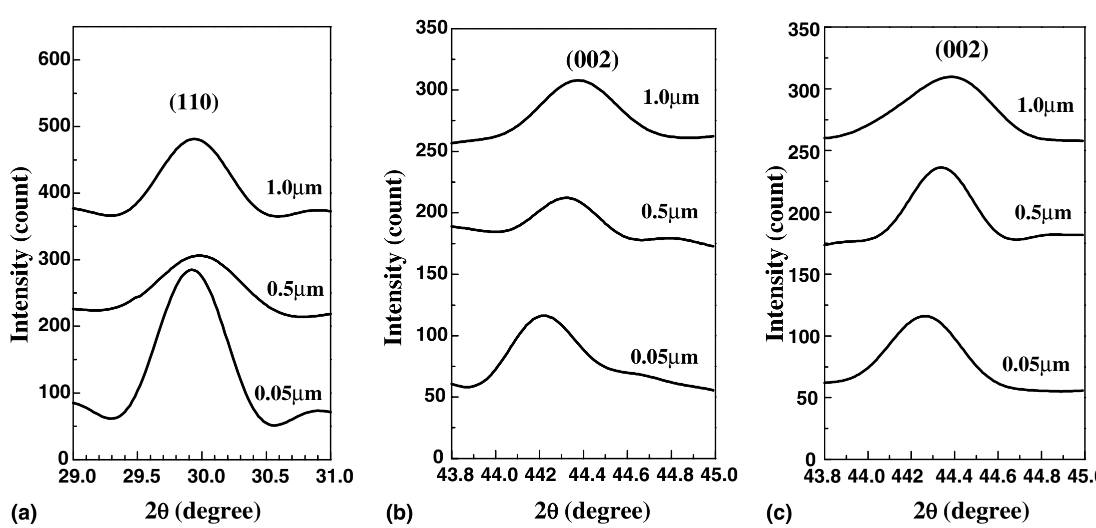

Fig. 4. XRD peaks of (a) PZT (1 1 0) plane before annealing, (b) PZT (0 0 2) plane before annealing, and (c) PZT (0 0 2) plane after annealing for PZT thin film with different thickness.

were calculated by extrapolation method and the results are listed in Table 2.

The representative SEM micrographs of PZT thin film with different thickness are shown in Fig. 5. It is obvious that the density variation of the tiny white spots indicates the phase transition between the trigonal and the tetragonal phase, and the amount of each phase is close because of the ratio of Zr/Ti = 52/48 in the sosoloid solid solution of binary system $PbZrO_3$–$PbTiO_3$. However, one cannot identify which phase the tiny white spots belong to from the SEM micrographs. On the other hand, the increase of crystal grain size with film thickness is visible.

4.2. Residual stress evaluated by XRD

The incidence angle of X-ray is adopted as $\psi = 0°$, 15°, 30° and 45°, and the diffraction spectrum for PZT thin film with different thickness is shown in Fig. 6. Taking $2\theta_\psi$ and $\sin^2\psi$ as ordinate and abscissa axis, the XRD data are plotted in Fig. 7 and the slope of $2\theta_\psi - \sin^2\psi$ straight line is obtained by the least square approximation. The relationship between $\sin^2\psi$ and the corresponding $2\theta_\psi$ is linearly simulated using the ORIGIN standard software and the results are listed in Table 3. According to the materials parameters given in Tables 1–3, the extended model described by equation (18) was used to evaluate the residual stress in PZT thin films with different thickness. On the other hand, the residual stress was also evaluated by the conventional model [6], in which the piezoelectric coupling effects are neglected. Fig. 8 shows the residual stresses in PZT thin films with thickness of 0.05, 0.5, and 1.0 μm are different, and the residual compress stresses in PZT thin films evaluated by the extended model are larger than those evaluated by the conventional model. It indicates that the conventional XRD measurement of residual stress may be inappropriate for the design and analysis of

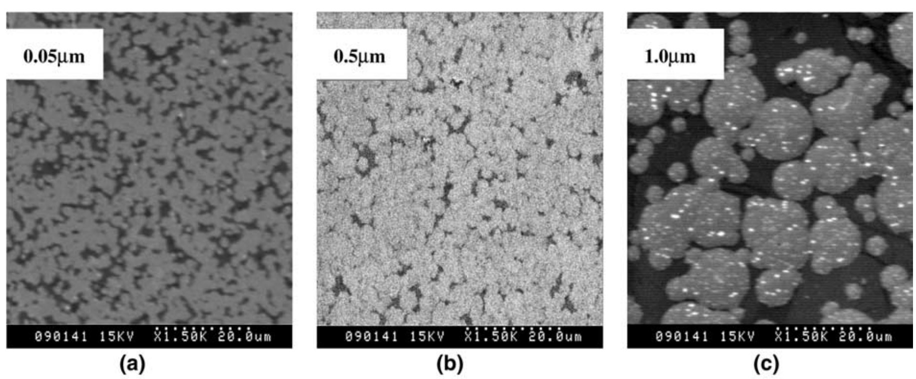

Fig. 5. Surface morphology of PZT films with different film thickness after HCL erodent: (a) 0.05 μm, (b) 0.5 μm, (c) 1.0 μm.

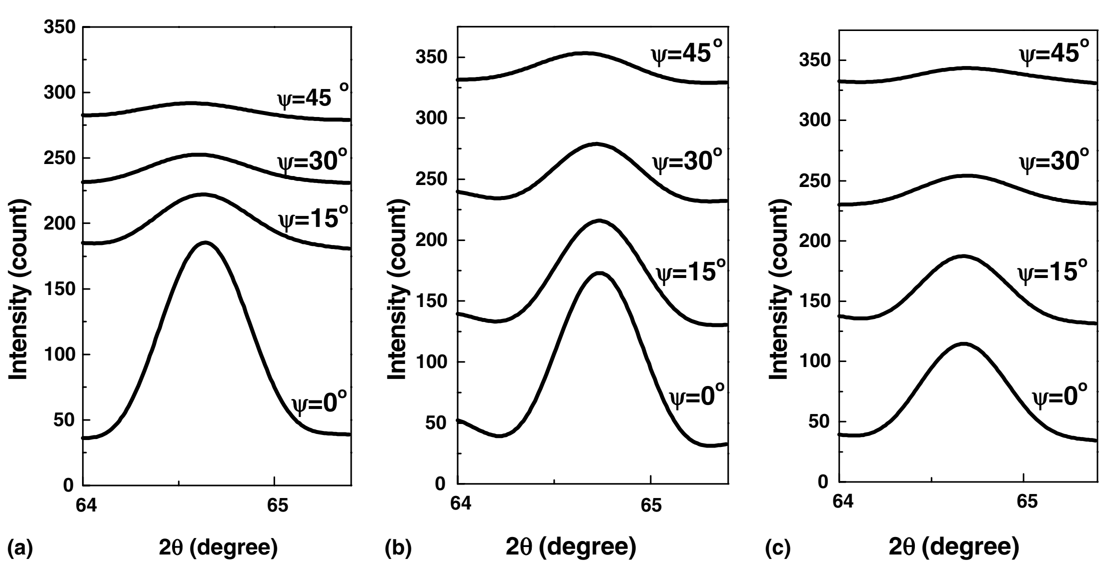

Fig. 6. XRD peaks of PZT (2 0 2) plane for three types of film thickness with different X-ray incident angles ψ: (a) 0.05 μm, (b) 0.5 μm, (c) 1.0 μm.

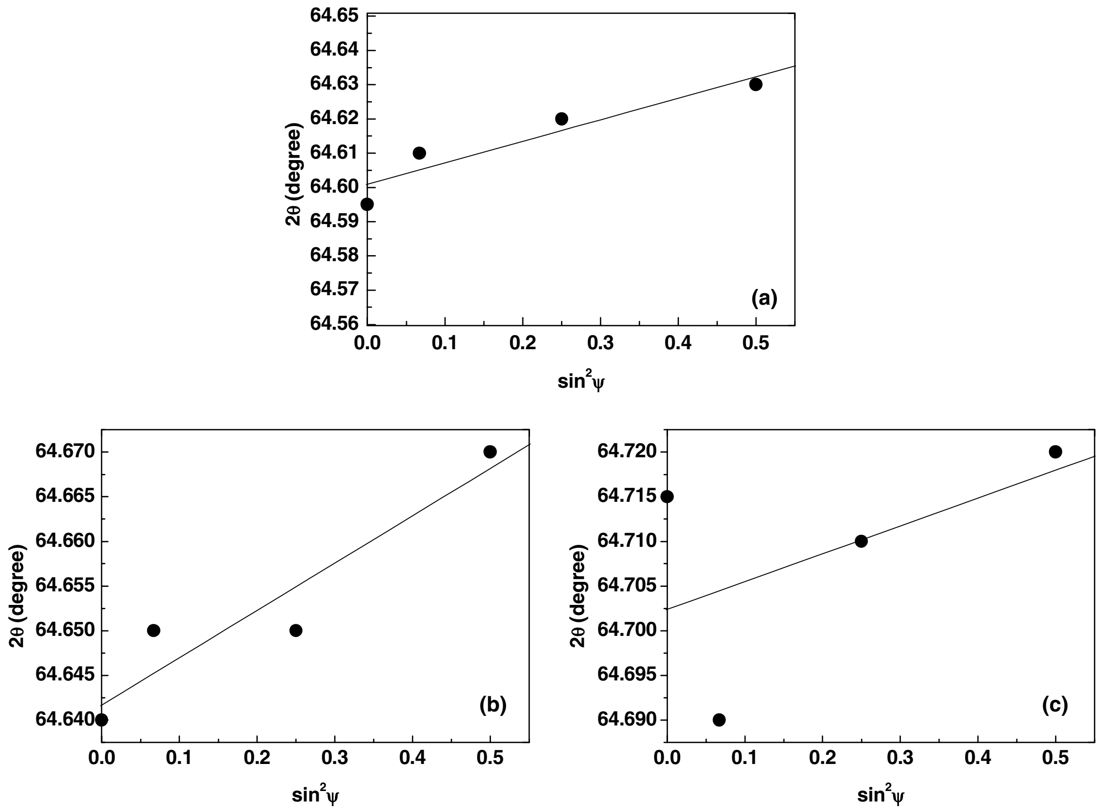

Fig. 7. Plots of $2\theta_{\psi} - \sin^2\psi$ for PZT thin films with different thickness (a) 0.05 μm, (b) 0.5 μm, and (c) 1.0 μm.

Table 3
The related diffraction angle with different incident X-ray angles

2θ	$\psi = 0°$	$\psi = 15°$	$\psi = 30°$	$\psi = 45°$	$\partial(2\theta)/\partial(\sin^2\psi)$
$h_1 = 0.05$ μm	64.595°	64.610°	64.620°	64.630°	0.063
$h_2 = 0.5$ μm	64.640°	64.650°	64.650°	64.670°	0.053
$h_3 = 1.0$ μm	64.715°	64.690°	64.700°	64.720°	0.028

ferroelectric thin film system, because the contribution of piezoelectric coupling on the residual stress has been neglected in the conventional model.

4.3. Origin of residual stress

In the preparation of laser beam ablation, PZT target materials were melted and vaporized. The melting and vaporous materials were deposited on the substrate by reverse impulse. During the film deposition at elevated temperature, strain due to misfit between the film and substrate would be developed. According to the minimum energy principium, there are four stresses in thin films, i.e., epitaxial stress σ_{ep}, intrinsic stress σ_{in}, thermal stress σ_{th} and transformation stress σ_{tr} [11,12]. The total residual stress σ_{res} in deposited thin film could be written as

$$\sigma_{res} = \sigma_{ep} + \sigma_{in} + \sigma_{th} + \sigma_{tr}. \quad (20)$$

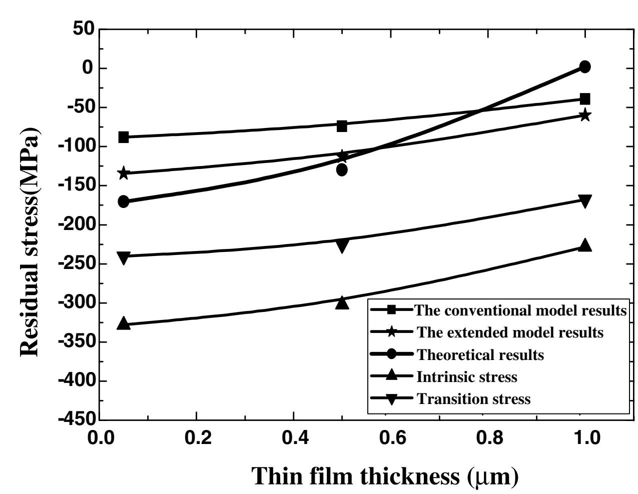

Fig. 8. The residual stress in PZT thin film: the results from conventional model (calculated in [6,27]); the results from extend model (in this paper); and the theoretical results (intrinsic stress from Eq. (21) and transition stress from Eq. (24)).

Since epitaxial strain develops at the growth temperature, it is reasonable that structural relaxation mechanisms should be active to relieve this stress. Therefore, epitaxial stress does not contribute to residual stress [11,25].

The difference of the c-axis lattice parameters before and after the annealing process was used to calculate the intrinsic stress as

$$\sigma_{\mathrm{in}} = -\frac{E_{\mathrm{f}}}{2v_{\mathrm{f}}}\frac{[A(c)_{\mathrm{f}} - B(c)_{\mathrm{f}}]}{B(c)_{\mathrm{f}}}, \tag{21}$$

where $A(c)_{\mathrm{f}}$ and $B(c)_{\mathrm{f}}$ are the c-axis lattice parameters of PZT thin film in tetragonal phase at room temperature, after and before annealing, respectively. At the film deposition temperature (T = 650 °C), the lattice parameter of cubic PZT is 4.05 Å [21] and that of Pt is estimated to be 3.95 Å [22]. Therefore, the lattice mismatch in this case, 2.5%, would result in compressive intrinsic stress. The intrinsic stresses for different film thickness could be easily calculated by Eq. (21), and the results are given in Fig. 8.

The thermal stress induced by the difference of thermal expansion coefficients between PZT thin film and substrate during cooling after deposition can be written as

$$\sigma_{\mathrm{th}} = \frac{E_{\mathrm{f}}}{(1-v_{\mathrm{f}})}\{[(\alpha(c)_{\mathrm{f}} - \alpha_{\mathrm{s}})](T_{\mathrm{s}} - T_{\mathrm{tr}}) + [(\alpha(t)_{\mathrm{f}} - \alpha_{\mathrm{s}})](T_{\mathrm{tr}} - T_0)\}, \tag{22}$$

where $\alpha(c)_{\mathrm{f}}$ and $\alpha(t)_{\mathrm{f}}$ are the thermal expansion coefficients of PZT thin film in the basal plane for the cubic and tetragonal phases, and they are assumed as 7.0×10^{-6}/K. α_{s} is the thermal expansion coefficient of the substrate and is taken as 3.5×10^{-6}/K. T_{s}, T_{tr} and T_0 are deposition temperature, phase transition temperature and room temperature, respectively. During the cooling from the growth temperature, PZT thin film undergoes a ferroelectric phase transition from a cubic phase to a tetragonal phase at 370 °C [26]. In the case of PZT thin film deposited on Si substrate, it is known that tensile stress is produced, and thermal stress about 0.398 GPa is not dependent on film thickness.

If the PZT films consist of only c- and a-domains, the phase transition stress can be expressed as in [6,12,27]. However, the contribution of non-($0\,0\,l$) and -($h\,0\,0$) area to the phase transition stress should be considered for the polycrystalline PZT films. The contribution of different orientation area to the phase transition stress generated along the principal x-axis σ_{tr} can be calculated using the elasticity theory. Using the stress analysis of Mohr's circle [12,28], the phase transition stress $\sigma_{\mathrm{tr}}^{(k\,l\,m)}(x)$ for each perfect orientation area can be written as

$$\begin{aligned}
&\alpha_{(k\,l\,m)} \neq 45°,\\
&\sigma_{\mathrm{tr}}^{(k\,l\,m)}(x) = \frac{E_{\mathrm{f}}}{(1-v_{\mathrm{f}})}\cdot\frac{[2a_0 - a(T) - c(T)]}{2a_0}\cdot\frac{\cos 4\alpha_{(k\,l\,m)}}{\cos^2 2\alpha_{(k\,l\,m)}}\\
&\qquad + \frac{E_{\mathrm{f}}}{(1+v_{\mathrm{f}})}\cdot\frac{[c(T) - a(T)]}{2a_0\cos 2\alpha_{(k\,l\,m)}},\\
&\alpha_{(k\,l\,m)} = 45°,\\
&\sigma_{\mathrm{tr}}^{(k\,l\,m)}(x) = \frac{E_{\mathrm{f}}}{(1-v_{\mathrm{f}})}\cdot\frac{[2a_0 - a(T) - c(T)]}{2a_0},
\end{aligned} \tag{23}$$

where $\alpha_{(k\,l\,m)}$ are determined as 0°, 45°, 90°, 26.6°, 65.9°, and 45° corresponding to (1 0 0), (1 1 0), (0 0 2), (2 0 1), (1 1 2) and (2 0 2)-oriented area. Using Eq. (23), the phase transition stress $\sigma_{\mathrm{tr}}^{(k\,l\,m)}(x)$ for the perfect a-domain, c-domian, non-($0\,0\,l$) and -($h\,0\,0$) area can be calculated and the results are listed in Table 4 in which the positive means tensile stress. Considering each population of the mixed domain structure corresponding to the ($k\,l\,m$)-oriented areas, the phase transition stress along the principal x-axis can be evaluated with the following equation:

$$\sigma_{\mathrm{tr}} = \sum_{i=1}^{6} P_{(k\,l\,m)}\sigma_{\mathrm{tr}}^{(k\,l\,m)}(x). \tag{24}$$

According to the parameters given in Tables 2 and 4, the phase transition stress σ_{tr} can be calculated by Eqs. (23) and (24), and the results are given in Table 4 and Fig. 8.

4.4. Residual stress of PZT thin films

According to Eq. (20), the total residual stress can be calculated and the result was described as "the theoretical result" in Fig. 8. It clearly indicates that the differences of evaluated residual stress by conventional method and extended method are about 20–50 MPa. The consideration of piezoelectric effect in the extended model described as Eq. (18) results in the differences, therefore one can conclude that the piezoelectric coupling factor defined as Eq. (17) plays an important role in the determination of residual stress in ferroelectric thin film. In fact, if the piezoelectric effect of PZT thin film is ignored, the piezoelectric coupling factor will

Table 4
The contribution of different orientation area to the phase transition stress (GPa)

	$P_{(1\,0\,0)}/\sigma_{\mathrm{tr}}^{(1\,0\,0)}$	$P_{(1\,1\,0)}/\sigma_{\mathrm{tr}}^{(1\,1\,0)}$	$P_{(0\,0\,2)}/\sigma_{\mathrm{tr}}^{(0\,0\,2)}$	$P_{(2\,0\,1)}/\sigma_{\mathrm{tr}}^{(2\,0\,1)}$	$P_{(1\,1\,2)}/\sigma_{\mathrm{tr}}^{(1\,1\,2)}$	$P_{(2\,0\,2)}/\sigma_{\mathrm{tr}}^{(2\,0\,2)}$	σ_{tr}
$h_1 = 0.05$ μm	20.07%/0.221	25.4%/−0.592	12.18%/−1.404	13.58%/1.823	10.96%/−1.070	15.81%/−0.592	−0.240
$h_2 = 0.5$ μm	15.89%/0.359	20.39%/−0.347	19.74%/−1.051	13.14%/1.449	14.14%/−0.971	16.69%/−0.347	−0.226
$h_3 = 1.0$ μm	10.83%/0.829	23.20%/0.030	22.15%/−0.769	10.84%/1.310	19.93%/−1.206	14.06%/0.030	−0.168

become elastic constant and the extended model will recover to the conventional model. Comparing the theoretical results with the experimental results evaluated by the conventional and extended models, the large absolute error is about ± 90 MPa for the former one while the absolute errors are ± 55 MPa for the latter one. It indicates that the piezoelectric effect of ferroelectric materials should not be ignored and using the extended method to evaluate residual stresses of ferroelectric thin film is necessary. Even though the extended method is used to evaluate residual stresses of PZT thin film, the large error exists. The large errors may be due to the small 2θ angle in XRD measurement. However, it is difficult to observe diffraction occurred at a larger diffraction angle in the present XRD technique. Therefore, improving measurement method and enhancing precision are key works for the accurate XRD stress measurement. On the other hand, the theoretical results are very sensitive to the materials parameters such as the elastic modulus, Poisson's ratio and thermal expansion coefficients of PZT thin films. However, the approximation that the materials parameters of PZT thin film do not vary with the film thickness is used in the calculation of theoretical residual stress. It may be another primary origin of the large errors for the calculation of residual stress.

5. Conclusions

We proposed an extended model taking into account the piezoelectric coupling effects to measure the residual stress in ferroelectric thin films with X-ray diffraction technique. Based on piezoelectric constitutive relationship and Bragg diffraction equation, the residual stresses were related to the slope $\partial(2\theta)/\partial(\sin^2\psi)$ of straight line $2\theta - \sin^2\psi$ and the coupling factor in terms of the elastic, dielectric and piezoelectric constants. The residual stresses of PZT thin films deposited by PLD were measured by D500 texture goniometer with the extended model and conventional model, respectively. The experimental results show the residual compressive stress evaluated by the former one is stronger than that evaluated by the latter one due to the piezoelectric coupling effects of PZT thin films. According to the minimum energy principium, the origin of residual stress was theoretically discussed from the stress contribution to the total free energy. The analytical results are close to the experimental results of the extended model.

Acknowledgements

We gratefully acknowledge the support of NNSF of China (No. 10072052), Trains-Century Training Program Foundation for the Talents by the State Education Commission of China (No. [2002]48), and Department Education of Hunan Province (No. 0313038).

Appendix A

Substituting the first two equations of Eqs. (8) into Eq. (7), we obtain

$$\begin{aligned}\sigma_\phi &= (c_{11}\varepsilon_1 + c_{12}\varepsilon_2)\cos^2\phi + (c_{12}\varepsilon_1 + c_{11}\varepsilon_2)\sin^2\phi \\ &\quad + (c_{13}\varepsilon_3 - e_{31}E_z) \\ &= c_{11}\varepsilon_1\cos^2\phi + c_{12}\varepsilon_1\sin^2\phi + c_{12}\varepsilon_2\cos^2\phi \\ &\quad + c_{11}\varepsilon_2\sin^2\phi + (c_{13}\varepsilon_3 - e_{31}E_z) \\ &= c_{11}\varepsilon_1\cos^2\phi + c_{12}\varepsilon_1(1-\cos^2\phi) + c_{12}\varepsilon_2(1-\sin^2\phi) \\ &\quad + c_{11}\varepsilon_2\sin^2\phi + (c_{13}\varepsilon_3 - e_{31}E_z) \\ &= (c_{11} - c_{12})(\varepsilon_1\cos^2\phi + \varepsilon_2\sin^2\phi) + c_{12}(\varepsilon_1 + \varepsilon_2) \\ &\quad + (c_{13}\varepsilon_3 - e_{31}E_z).\end{aligned} \tag{A.1}$$

Eqs. (10) and (11) are substituted into Eq. (A.1), resulting in

$$\begin{aligned}\sigma_\phi &= (c_{11} - c_{12})(\varepsilon_1\cos^2\phi + \varepsilon_2\sin^2\phi) \\ &\quad - \frac{c_{12}(c_{33}\epsilon_{33} + e_{33}^2)}{(c_{13}\epsilon_{33} + e_{31}e_{33})}\varepsilon_3 + c_{13}\varepsilon_3 - \frac{e_{31}(c_{33}e_{31} - e_{33}c_{13})}{(e_{33}e_{31} + c_{13}\epsilon_{33})}\varepsilon_3 \\ &= (c_{11} - c_{12})(\varepsilon_1\cos^2\phi + \varepsilon_2\sin^2\phi) \\ &\quad - \frac{c_{12}(c_{33}\epsilon_{33} + e_{33}^2) + e_{31}^2c_{33} - 2c_{13}e_{31}e_{33} - c_{13}^2\epsilon_{33}}{c_{13}\epsilon_{33} + e_{31}e_{33}}\varepsilon_3.\end{aligned} \tag{A.2}$$

Reforming Eq. (A.2), Eq. (12) can be derived.

Appendix B

Adding the first two equations of Eqs. (8) yields

$$\sigma_1 + \sigma_2 = (c_{11} + c_{12})(\varepsilon_1 + \varepsilon_2) + 2(c_{13}\varepsilon_3 - e_{31}E_z). \tag{B.1}$$

Substituting Eqs. (10) and (11) into Eq. (B.1), one can obtain

$$\begin{aligned}\sigma_1 + \sigma_2 &= -\frac{(c_{11} + c_{12})(c_{33}\epsilon_{33} + e_{33}^2)}{(c_{13}\epsilon_{33} + e_{31}e_{33})}\varepsilon_3 + 2c_{13}\varepsilon_3 \\ &\quad - \frac{2e_{31}(c_{33}e_{31} - e_{33}c_{13})}{(e_{33}e_{31} + c_{13}\epsilon_{33})}\varepsilon_3 \\ &= [4c_{13}e_{31}e_{33} + 2c_{13}^2\epsilon_{33} - 2e_{31}^2c_{33} \\ &\quad - (c_{11} + c_{12})(c_{33}\epsilon_{33} + e_{33}^2)]/(c_{13}\epsilon_{33} + e_{31}e_{33})\varepsilon_3.\end{aligned} \tag{B.2}$$

Appendix C

Substituting Eq. (15) into Eq. (B.2), one can obtain

$$\begin{aligned}\sigma_1 = \sigma_2 &= \sigma_\phi \\ &= [4c_{13}e_{31}e_{33} + 2c_{13}^2\epsilon_{33} - 2e_{31}^2c_{33} - (c_{11} + c_{12}) \\ &\quad \times (c_{33}\epsilon_{33} + e_{33}^2)]/[2(c_{13}\epsilon_{33} + e_{31}e_{33})]\varepsilon_3.\end{aligned} \tag{C.1}$$

Then

$$\frac{\varepsilon_3}{(c_{13}\epsilon_{33} + e_{31}e_{33})} = (2\sigma_\phi)/[4c_{13}e_{31}e_{33} + 2c_{13}^2\epsilon_{33} - 2e_{31}^2c_{33} - (c_{11} + c_{12})(c_{33}\epsilon_{33} + e_{33}^2)]. \tag{C.2}$$

Substituting Eq. (C.2) into the right-hand side of Eq. (13), one can obtain

$$\begin{aligned}\frac{(c_{11}-c_{12})(\varepsilon_{\phi\psi}-\varepsilon_3)}{\sin^2\psi} &= \sigma_\phi + [c_{12}(c_{33}\epsilon_{33}+e_{33}^2)+e_{31}^2c_{33}-2c_{13}e_{31}e_{33}-c_{13}^2\epsilon_{33}] \\ &\quad /[c_{13}\epsilon_{33}+e_{31}e_{33})-c_{11}+c_{12}]\varepsilon_3 \\ &= \sigma_\phi + [c_{12}(c_{33}\epsilon_{33}+e_{33}^2)+e_{31}^2c_{33}-2c_{13}e_{31}e_{33}-c_{13}^2\epsilon_{33} \\ &\quad +(c_{12}-c_{11})(c_{13}\epsilon_{33}+e_{31}e_{33})] \\ &\quad /[4c_{13}e_{31}e_{33}+2c_{13}^2\epsilon_{33}-2e_{31}^2c_{33}-(c_{11}+c_{12})(c_{33}\epsilon_{33}+e_{33}^2)]2\sigma_\phi \\ &= [(c_{12}-c_{11})(c_{33}\epsilon_{33}+e_{33}^2)+2(c_{12}-c_{11})(c_{13}\epsilon_{33}+e_{31}e_{33})] \\ &\quad /[4c_{13}e_{31}e_{33}+2c_{13}^2\epsilon_{33}-2e_{31}^2c_{33}-(c_{11}+c_{12})(c_{33}\epsilon_{33}+e_{33}^2)]\sigma_\phi.\end{aligned} \tag{C.3}$$

Divide Eq. (C.3) by the factor $(c_{11} - c_{12})$, one can obtain

$$\begin{aligned}\sigma_\phi &= [(c_{11}+c_{12})(c_{33}\epsilon_{33}+e_{33}^2)-4c_{13}e_{31}e_{33}-2c_{13}^2\epsilon_{33}+2e_{31}^2c_{33}] \\ &\quad /[2(c_{13}\epsilon_{33}+e_{31}e_{33})+(c_{33}\epsilon_{33}+e_{33}^2)]\frac{(\varepsilon_{\phi\psi}-\varepsilon_3)}{\sin^2\psi}.\end{aligned} \tag{C.4}$$

References

[1] Haertling GH. J Am Ceram Soc 1999;82:797.
[2] Scott JF, Araujo CAP. Science 1989;246:1400.
[3] Alguero MA, Bushby J, Reece MJ, Seifert A. Appl Phys Lett 2002;81:421.
[4] Bahr DF, Robach JS, Wright JS, Francis LF, Gerberich WW. Mater Sci Eng A 1999;259:126.
[5] Zheng XJ, Zhou YC, Li JJ. Acta Mater 2003;51:3985.
[6] Zheng XJ, Yang ZY, Zhou YC. Scr Mater 2003;49:71.
[7] Fuji T, Watanabe S, Suzuki M, Fujiu T. J Vac Sci Technol B 1995;13:1119.
[8] Maeder T, Muralt P, Sagalowicz L, Reaney I, Kohli M, Kholkin A, et al. Appl Phys Lett 1996;68:776.
[9] Fu HX, Cohen RE. Nature 2000;403:281.
[10] Chen HD, Udayakumar KR, Gaskey CJ, Cross LE. Appl Phys Lett 1995;67:3411.
[11] Sakashita Y, Segawa H. J Appl Phys 1993;73:7857.
[12] Kweon SY, Yi SH, Choi SK. J Vac Sci Technol A 1997;15:57.
[13] Hutchinson JW, Suo Z. Adv Appl Mech 1992;29:63.
[14] Evans AG, Hutchinson JW. Acta Metall Mater 1995;43:2507.
[15] Xu WH, Lu D, Zhang TY. Appl Phys Lett 2001;79:4112.
[16] Sandeep K, Christopher DR, Peter KD. J Appl Phys 2002;91:1149.
[17] Gergaud P, Thomas O, Chenevier B. J Appl Phys 2003;94:1584.
[18] Suresh S, Giannakopoulos AE. Acta Mater 1998;46:5755.
[19] Thielsch R, Hassler W, Bruckner W. Phys Stat Sol (a) 1996;156:199.
[20] Shirane G, Suzuki K, Takeda A. J Phys Soc Jpn 1952;7:12.
[21] Xu YH. Ferroelectric materials and their applications. Amsterdam: North-Holland; 1991. p. 109.
[22] Kobbin PH, Harker AB. J Mater Sci 1989;24:1363.
[23] Floquet N, Hector J, Gaucher P. J Appl Phys 1998;84:3815.
[24] Sakashita Y, Ono T, Segawa H, Tominaga K, Okada M. J Appl Phys 1991;69:8352.
[25] Foster CM, Li Z, Buckett M, et al. J Appl Phys 1995;78:2607.
[26] Nakamura E, Mitsui T. In: Complex perovskite-type oxide, Landolt–Bornstein: oxides, vol. 28. Berlin: Springer; 1990.
[27] Zhou YC, Yang ZY, Zheng XJ. Surf Coat Technol 2003;162:202.
[28] Speck JS, Daykin AC, Seifert A. J Appl Phys 1995;78:1696.